AGU PUBLICATIONS

Water Resources Research

RESEARCH ARTICLE
10.1002/2014WR016623

# Temporal responses of groundwater-surface water exchange to successive storm events

**Marina Dudley-Southern[1] and Andrew Binley[1]**

[1]Lancaster Environment Centre, Lancaster University, Lancaster, UK

**Key Points:**
- Hyporheic zone is temporarily expanded due to storm events
- Short-lived downwelling during events may fuel biogeochemical processes
- Electrical conductivity is highlighted as a tracer of hyporheic travel times

**Correspondence to:**
A. Binley,
a.binley@lancaster.ac.uk

**Citation:**
Dudley-Southern, M., and A. Binley (2015), Temporal responses of groundwater-surface water exchange to successive storm events, *Water Resour. Res.*, *51*, 1112–1126, doi:10.1002/2014WR016623.

Received 3 NOV 2014
Accepted 22 JAN 2015
Accepted article online 28 JAN 2015
Published online 23 FEB 2015

**Abstract** Groundwater-surface water exchange within the hyporheic zone is widely recognized as a key mechanism controlling the fate of nutrients within catchments. In gaining river systems, groundwater-surface water interactions are constrained by upwelling groundwater but there is increasing evidence that a rapid rise in river stage during storm events can result in a temporary reversal of vertical hydraulic gradients, leading to surface water infiltration into the subsurface and supply of surface-borne reactive solutes to this biogeochemically active interface. At a UK study site, using logged hydraulic heads in the surface water, riverbed, and riverbanks and logged electrical conductivity at multiple depths in the riverbed we show that storm events can lead to a temporary reversal of vertical hydraulic gradient with mixing evident up to 30 cm beneath the riverbed. Cross-channel variability is evident, with the center of the channel consistently having shorter reversals of hydraulic gradient, compared to the channel margins. The direction of shallow subsurface riverbank flow at the site is also reactive to storm events, temporarily aligning with the surface flow direction and then reverting back to preevent conditions. Such a transition of flow paths during events is also likely to lead to expansion of lateral hyporheic exchange. This study provides evidence that storm events can be a key driver of enhanced hyporheic exchange in gaining river systems, which may support nutrient reactions beyond the duration of event-driven change. Our observations demonstrate the dynamic nature of the hyporheic zone, which should be considered when evaluating its biogeochemical function.

## 1. Introduction

The hyporheic zone, where surface water and groundwater mix, is recognized as a hotspot of biogeochemical cycling [*McClain et al*., 2003], which can have a significant control on the fate of nutrients within a catchment. Rates of nitrogen transformation processes are often increased within the hyporheic zone and the distinction between net nitrification or net denitrification is dependent on the residence time of water within the hyporheic zone [*Zarnetske et al*., 2011], as well as the availability of reactants, principally labile dissolved organic carbon [*Baker et al*., 1999].

Hyporheic exchange flow (HEF) is the process by which stream water infiltrates into the streambed or the stream banks and returns to the stream over relatively short distances or times [*Harvey et al*., 1996].While the physical controls on HEF have been intensively studied in recent years, the temporal dynamics of flow and solute transport has received relatively little attention [*Krause et al*., 2014] and few field studies have directly estimated changes in hyporheic zone mixing depth and timescales of exchanges under fluctuating stream conditions [*Gerecht et al*., 2011]. Temporal variability in hyporheic exchange and the mixing depth between surface water and groundwater can drive hot moments of biogeochemical cycling within the hyporheic zone, where episodic flow paths mobilize reactants and reactivate microbial communities [*McClain et al*., 2003]. This can be particularly important in gaining river systems, where upwelling groundwater can limit the extent of the hyporheic zone [*Boano et al*., 2008].

Several field studies focusing on nonsteady state dynamics have considered dam operations for hydropower generation that result in consistent and replicated changes to river stage [*Arntzen et al*., 2006; *Fritz and Arntzen*, 2007; *Gerecht et al*., 2011; *Sawyer et al*., 2009]. Other studies have evaluated the impact of variable river stage around in-stream structures such as beaver dams [*Briggs et al*., 2012] and within salmon spawning gravels [*Malcolm et al*., 2006; *Malcolm et al*., 2004]. Relatively few studies have considered storm event-induced changes on groundwater-surface water interactions and have been limited to daily sampling

over the course of a large event [*Zimmer and Lautz*, 2014], repeated point sampling [*Sawyer et al*., 2014], and comparisons between low and high flows [*Byrne et al*., 2014]. Riverbed pore water chemistry is rarely reported under peak flow conditions due to safety considerations during sampling [*Zimmer and Lautz*, 2014; *Malcolm et al*., 2004; *Sawyer et al*., 2014], therefore missing a key period in event-driven changes and preventing the calculation of lag times in responses to peak flows at multiple locations [*Sawyer et al*., 2014]. It has been highlighted that characterization of the hyporheic zone needs to move beyond point descriptions to understanding of processes integrated through space and time [*Briggs et al*., 2012]. This has been reflected in a move away from studies based on a few days of observations [*Arntzen et al*., 2006; *Gerecht et al*., 2011; *Sawyer et al*., 2009] to month long records [*Briggs et al*., 2012] and further extended periods of observations. Another key area for development of nonsteady state field investigations is to include transects across riverbeds, as it has been noted that significant variability in both flow paths and pore water chemistry can exist across a stream channel; studies focused on measurements in the center of the channel may underestimate the impact of storm events [*Gerecht et al*., 2011], as groundwater flux may be focused through the center of the channel [*Genereux et al*., 2008; *Kennedy et al*., 2009].

This work forms part of a larger "parent" project investigating groundwater-surface water interactions and implications for nitrogen transformations in a gaining river reach of the River Leith, Cumbria, UK. The River Leith is part of the Eden catchment in which groundwater nitrate concentrations are rising as a result of nitrogen applied to grassland, as slurry and inorganic fertilizers, in excess of crop nutrient requirements [*Butcher et al*., 2003]. Previous hydrological and biogeochemical investigations at the study site have focused on base flow conditions [*Binley et al*., 2013; *Heppell et al*., 2014; *Lansdown et al*., 2014] and have identified an area of preferential groundwater discharge in the upstream part of the site that limits the vertical extent of the hyporheic zone under low flow conditions. The control of upwelling groundwater on the extent of the hyporheic zone has been seen in field studies [*Gerecht et al*., 2011; *Sawyer et al*., 2009] and modeling studies [*Boano et al*., 2008; *Cardenas and Wilson*, 2007] and has been shown to limit surface water infiltration, and consequently the delivery of organic matter to organisms in the subsurface [*Gerecht et al*., 2011], potentially reducing the nutrient attenuation capacity of the hyporheic zone. Under base flow conditions, a region of strong upwelling groundwater in the bed sediments of the River Leith has been characterized as oxic with high nitrate concentrations and low particulate organic matter content [*Heppell et al*., 2014]. In these regions, denitrification rates decline with increasing depth [*Lansdown et al*., 2012], leading to speculation that such patterns reflect the dependence of denitrification on organic matter derived from surface water inputs to the subsurface [*Holmes et al*., 1996; *Lansdown et al*., 2012; *Stelzer and Bartsch*, 2012]. In this study, we investigate a zone of preferential groundwater discharge in the River Leith, in order to assess the dynamics of HEF under storm events.

*Zimmer and Lautz* [2014] highlighted two main processes that are known to control subchannel hyporheic exchange under fluctuating stage conditions: (1) rapidly increased stage causes stream water influx into the riverbed or (2) hydraulic gradient toward the stream is increased as a result of aquifer recharge during precipitation events, reducing the vertical extent of the hyporheic zone. *Byrne et al*. [2014] previously investigated the effect of small changes in stage ($<$40 cm above low flow stage) at the River Leith site over a 4 month summer period. It was noted that in the upstream, constrained and incised subreach, vertical hydraulic gradients decreased under high stage conditions and the vertical extent of the hyporheic zone increased from less than 10 cm to 10 cm depth beneath the riverbed. This suggests that the first process described by *Zimmer and Lautz* [2014] is active at the upstream part of the field site and leads us to hypothesize that, in the gaining river reach rapid, large and repeated changes in stage will temporarily reduce vertical hydraulic gradients, allowing enhanced surface water downwelling. The main aim of this paper is to examine how vertical hydraulic gradients and mixing depths between surface water and groundwater, in a zone of preferential groundwater discharge, responds to high stage events and to derive the timescale of induced changes. The objectives of the study are to: (1) evaluate the stability of vertical hydraulic gradients over a prolonged time period at the study location; (2) examine the changes in vertical gradients and mixing depth across the riverbed, and the timescales of those changes; (3) demonstrate the use of electrical conductivity to explore hyporheic exchange; and (4) further develop a conceptual model of surface-subsurface mixing at the study site to include event-driven changes. Although our observations are site-specific, we believe that the general findings are not unique to this site.

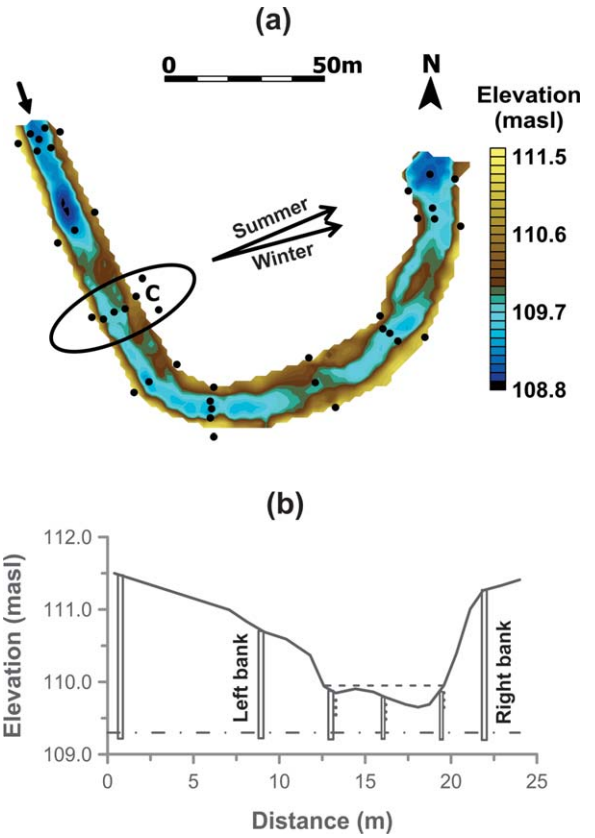


**Figure 1.** (a) River Leith 200 m meander reach riverbed topography (masl), modified from *Binley et al.* [2013]. Flow direction is denoted by the arrow and black circles represent channel and riparian piezometers. Circled area highlights sampling site C that is the focus of this study. Labeled arrows represent deep (50 m) groundwater mean flow bearing during summer and winter seasons between January 2005 and June 2011 (Environment Agency, personal communication, 2014) (b) Cross section of sampling site C indicating location of riverbed and riverbank piezometers, where dot-dash line marks depth of screened sections (0.5 m beneath riverbed). Black dots are location of electrical conductivity measurements beneath the riverbed. Dashed line marks minimum stage for the period May 2012 to January 2014. Note exaggerated elevation scale.

In this study, we use fluid electrical conductivity as a natural tracer signal, in order to provide evidence of event-based downwelling. Relatively few studies of groundwater-surface water interactions have used logged subsurface electrical conductivity [*Cirpka et al.*, 2007; *Schmidt et al.*, 2012; *Vogt et al.*, 2010] despite the fact that solute concentrations (expressed by electrical conductivity) are likely to propagate further into the subsurface and not undergo retardation, compared to temperature signals which are conducted through both the solids and water phases of the bulk sediment [*Cirpka et al.*, 2007; *Vogt et al.*, 2010]. Field studies using logged electrical conductivity have focused on determining travel-time distributions to pumping wells [*Cirpka et al.*, 2007] and bank infiltration along a losing stream [*Vogt et al.*, 2010], deriving lateral flow velocities in an in-stream gravel bar [*Schmidt et al.*, 2012], induced exchange across a stream meander [*Osenbrück et al.*, 2013] and identifying areas of gaining or losing conditions along a river reach [*Unland et al.*, 2013]. The above studies are all based on loggers in piezometers or boreholes and have not evaluated fluid electrical conductivity as a tracer of vertical mixing between groundwater and surface water beneath a riverbed.

Electrical resistivity imaging (ERI) methods have been used to produce 2-D images of the spatial variability of hyporheic exchange under low flow conditions [*Ward et al.*, 2012; *Ward et al.*, 2010b; *Ward et al.*, 2010a] and, more recently, have been used to examine temporal exchange dynamics, in dam-regulated rivers [*Cardenas and Markowski*, 2010; *Johnson et al.*, 2012]. However, most ERI studies require a large conservative solute tracer addition to the stream channel [*Ward et al.*, 2010b; *Ward et al.*, 2010a; *Ward et al.*, 2012], therefore eliminating long-term monitoring and evaluation under high stage conditions. The high concentrations needed also limit applications to small streams and environments where significant changes in stream chemistry are not considered detrimental to ecosystem health. Also, estimated changes in hyporheic extent are sensitive to the threshold level of signal change that is chosen to represent changes in bulk resistivity beyond the error in both data collection and modeling [*Ward et al.*, 2010b] and it is noted that ERI methods provide better data when tracer distributions are changing slowly, rather than in highly advective hyporheic flow paths [*Ward et al.*, 2010a].

Here we highlight the use of high-frequency logged fluid electrical conductivity at multiple depths beneath a riverbed, with the sensors in direct contact with the riverbed sediments and pore waters, as a responsive in situ method for monitoring an environmental tracer. Logged fluid electrical conductivity can be used in long duration field campaigns and throughout multiple events to examine changes in groundwater-surface water mixing depth. This addresses key gaps in the literature by estimating

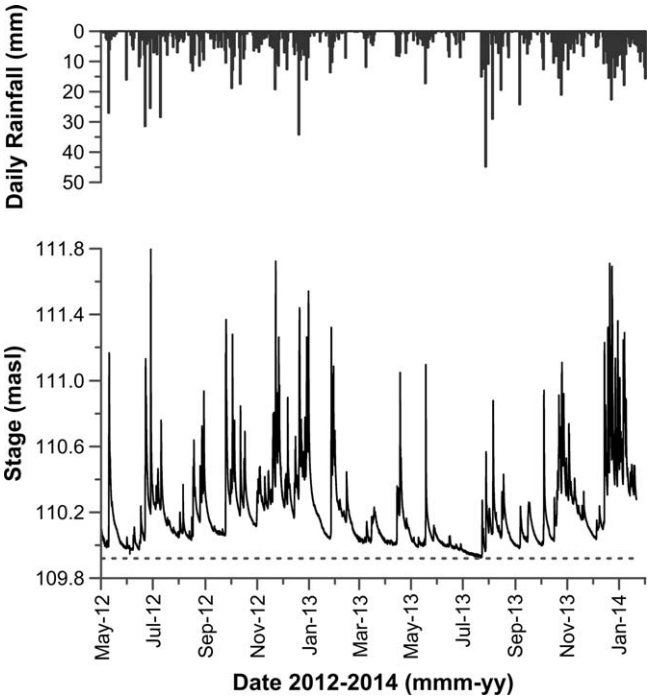


**Figure 2.** Daily rainfall (mm) (Environment Agency, personal communication, 2014) and stage (masl) from May 2012 to January 2014. Horizontal-dashed line marks minimum stage for the study period.

changes in vertical mixing depth and deriving corresponding advective velocities [*Gerecht et al.*, 2011] under a wide range of surface flow conditions [*Briggs et al.*, 2012].

## 2. Field Site and Methods

### 2.1. Study Site

This investigation is based on a 200 m meander reach of the River Leith (Figure 1), a tributary of the River Eden, Cumbria, UK. The River Eden controls the direction of groundwater flow which, expressed as a bearing, fluctuates by 5° between winter and summer periods (Figure 1). The River Leith catchment (54 km$^2$) lies on Permo-Triassic sandstone which is overlain by shallow (<2 m) glaciofluvial deposits. The channel morphology of the 200 m meander study reach (Figure 1) is made up of alternating riffle-pool sequences and has been identified as predominantly groundwater fed [*Käser et al.*, 2009].

### 2.2. Field Methods

The research undertaken here is concentrated within the upstream part of the reach, centered around sampling site C (Figure 1), and covers a 21 month period between May 2012 and January 2014, with a particular focus on a series of large magnitude (river stage increases greater than 1 m relative to the minimum stage for the period) storm events during December 2013 and early January 2014 (Figure 2). Sampling site C was identified as a preferential discharge location where, under low flow conditions, upwelling groundwater acts to suppress the extent of vertical hyporheic exchange [*Binley et al.*, 2013].

**Table 1.** Total Rainfall (mm) and Number of Events Resulting in an Increase in Stage Greater Than 1 m Relative to Minimum Stage for the Period May 2012 and January 2014 (109.92 masl), by Season

| Season[a] | Total Rainfall (mm) | Number of Events Where Stage Increased by More Than 1 m Relative to Minimum Stage |
|---|---|---|
| Spring 2012 | 136.2 | 1[b] |
| Summer 2012 | 306.4 | 3 |
| Autumn 2012 | 255.4 | 5 |
| Winter 2012 | 233.0 | 6 |
| Spring 2013 | 130.0 | 2 |
| Summer 2013 | 228.4 | 0 |
| Autumn 2013 | 236.6 | 4 |
| Winter 2013 | 439.2 | 11[c] |

[a]Seasons are defined as Spring: March–May; Summer: June–August; Autumn: September–November; Winter: December–February.
[b]Spring 2012 event data covered May 2012 only.
[c]Winter 2013 event data covered 1 December 2013 to 22 January 2014 only.

Rainfall data recorded by a tipping bucket rain gauge at Kirkby Thore near Penrith (N54:37:30; W2:33:37), approximately 5 km East of the study reach, were provided by the Environment Agency of England and Wales. The yearly total rainfall during 2012 and 2013 were similar: 931 and 1034 mm, respectively, resulting in frequent high stage events throughout the monitored period (Figure 2). Spring (March–May inclusive) was the driest season in both years and rainfall was spread evenly throughout 2012 (Table 1). 40% of the total rainfall in 2013 fell in winter (December–January inclusive), leading to a prolonged period of elevated stage conditions (Figure 2).The maximum daily rainfall recorded was 44.8 mm on 28 July 2013 and the minimum recorded stage for the period (109.92 masl) coincided with the end of 20 day period with no rainfall between 3 July 2013 and 22 July 2013. The maximum stage was 111.8 masl, recorded on 28 June 2012 (Figure 2).

Focusing on the 7 week period between 4 December 2013 and 22 January 2014, 132 mm of rainfall fell in the second 2 weeks of December, causing an extended period of high

stage conditions (Figure 2) with multiple high stage events (Table 1). River discharge data for December 2013 and January 2014 were logged at Cliburn Weir (N54:37:03; W2:38:23), approximately 50 m downstream of the study reach (data provided by the Environment Agency of England and Wales). At the beginning of December 2013, river discharge was characteristic of low flow conditions (mean daily river discharge 0.53 $m^3/s$). Throughout the duration of the storm events, river discharge exceeded the valid range of current rating for the weir; therefore, no discharge data were recorded. By the middle of January 2014, river discharge had reduced to a mean daily value of 2.07 $m^3/s$.

#### 2.2.1. Piezometers

As part of the wider parent project 87, 32 mm (outer) diameter, uPVC (unplasticized polyvinyl chloride) piezometers were installed in channel and riparian locations along the study reach in June 2009 and June 2010 (Figure 1) (for full details of piezometers refer to *Binley et al*. [2013]). Channel piezometers were installed in nests across the channel, with piezometers screened at 100, 50, and 20 cm depths beneath the riverbed. Riparian piezometers were installed on both banks to a depth of 50 cm below the adjacent riverbed elevation. A further two riparian piezometers were installed to a depth of 50 cm beneath the adjacent riverbed elevation on the left bank at site C in July 2013 (Figure 1) to enable the shallow groundwater riverbank flow direction to be determined by triangulation of head data.

#### 2.2.2. Hydrological Measurements

Pressure transducers (HOBO U20-001-01, Onset Computer Corporation, Bourne, MA, USA) were installed in pairs at the left, center, and right channel locations at sampling site C to record the piezometric head at 50 cm depth beneath the riverbed and the associated river stage, at 15 min intervals. Each subchannel piezometer had its own associated stage logger to negate the need to adjust stage levels between different measurement locations, maintaining a low uncertainty in subsequent vertical hydraulic gradient calculations [*Käser et al*., 2009]. Pressure transducers were also installed in the riparian piezometers to record the riparian piezometric head at 50 cm below the adjacent stream channel elevation. Pressure data were barometrically compensated and then calibrated, using discrete manual (dip) measurements of the hydraulic head at each piezometer and the local river water level adjacent to the piezometer, using a narrow diameter electronic dip meter. After calibration to the discrete measurements, the residual error between logged and dipped data was assumed to be $+/-0.25$ cm. In-stream vertical hydraulic gradients were calculated, as a percentage, using $100 \cdot dh/dl$, where dh is the elevation difference between the piezometric head and the stage adjacent to the piezometer, and dl is the vertical distance between the midscreen depth of the piezometer and the riverbed (throughout this paper dl is 50 cm). Here, we define a positive hydraulic gradient as the piezometric head exceeding the stage level i.e., there is potential for groundwater upwelling into the river. The left bank flow bearing and gradient was calculated by triangulation of the three riparian piezometric heads.

#### 2.2.3. Fluid Electrical Conductivity Measurements

Electrical conductivity in the surface water and at 10, 20, and 30 cm depths beneath the riverbed at the left, center, and right channel locations at sampling site C was logged using 4 electrode sensors from June 2013 to January 2014. The sensors were fabricated using 1.5 cm diameter solid polyvinyl chloride (PVC) rods with the center of the electrode array driven in to the riverbed to the required depth. To maintain a suitable anchor in the riverbed, in order to withstand disturbance by storm events, the total length of all sensor rods was 45 cm. Each four electrode sensor was constructed using 0.5 cm diameter stainless steel screws that were driven in to the PVC rod until the screw heads were flush with the outside of the rod. The stainless steel screws were separated by 0.5 cm, resulting in a total length of the sensor of 3.5 cm. Screened four core cable was wired to the four electrodes. The cable was recessed in to the rod and then held in place using a plastic casting resin. Each sensor was connected to a Campbell CR10X (Campbell Scientific Incorporated, Utah, USA) data logger which was programmed to log electrical conductance at 5 min intervals, using two electrodes to create a potential field and the other two electrodes to measure a potential gradient in a Wenner-type electrode configuration commonly used for direct current resistivity measurements [see, e.g., *Binley and Kemna*, 2005]. A four electrode design was adopted to minimize polarization, and hence deterioration, of electrodes.

Prior to installation in the field and after removal from the field, each sensor was calibrated in multiple solutions of known fluid electrical conductivity in order to determine an appropriate geometric factor (or cell constant) for each probe. As there was minimal change between calibrations before installation and after

removal from the field, a mean calibration was applied to each sensor for the duration of the logged period. Field measurements were corrected to 25°C after *Sorensen and Glass* [1987]:

$$EC_{25} = EC_T[1 + a(25 - T)], \quad (1)$$

where $EC_{25}$ is the electrical conductivity at 25°C, $EC_T$ is the electrical conductivity at temperature T (°C), and $\alpha$ is the temperature compensation factor ($^\circ C^{-1}$). Simultaneous temperature measurements were recorded at the left, center, and right channel locations at the same depths using thermocouples (TMC20-HD, Onset Computer Corporation, Bourne, MA, USA) in steel casings connected to four channel data loggers (HOBO U12-006, Onset Computer Corporation, Bourne MA, USA). A 2 %/°C temperature compensation factor was used which is suitable over the temperature range in the data series [*Hayashi*, 2004]. The calibrated field measurements recorded the effective (bulk) electrical conductivity. To obtain the fluid electrical conductivity from the effective electrical conductivity, assuming minimal impact of electrical conductance along the surface of the grains, Archie's law [*Archie*, 1942] was used:

$$\sigma_W = F\sigma_{eff}, \quad (2)$$

where, $\sigma_W$ is the fluid electrical conductivity, $\sigma_{eff}$ is the measured effective (bulk) conductivity, and $F$ is the electrical formation factor which is related to porosity ($n$) and the pore structure of the material ($m$; the cementation index) according to:

$$F = n^{-m} \quad (3)$$

A formation factor of 4.2 was used which was derived from an estimated porosity of 0.33 and cementation index value for unconsolidated sands of 1.3 [*Archie*, 1942]. Note that the assumed value of formation factor is not critical in the analysis that follows as we are concerned with the temporal changes in fluid conductivity, measured from the changes in bulk electrical conductivity over time.

### 2.3. Calculation of Infiltrating Surface Water Advective Velocity and Saturated Hydraulic Conductivity of Shallow Riverbed Sediments

It had been intended to use the time delay between the decrease in fluid electrical conductivity in the surface water and the decrease in fluid electrical conductivity at depths beneath the riverbed in response to events to obtain a travel time of surface water in to the subsurface; however, biofilm development on the surface water electrodes prevented reliable data collection. Assuming surface water infiltration into the riverbed as a result of negative vertical hydraulic gradients moving as a front of water through all pore spaces, the vertical distance between the riverbed and subsurface electrode divided by the time delay between the onset of the negative vertical hydraulic gradient and the initial decrease in fluid electrical conductivity can instead be used to derive an advective velocity of surface water infiltration into the subsurface. Advective velocities between fluid electrical conductivity responses at multiple depths in the subsurface were calculated by dividing the vertical distance between the electrodes by the time delay between the initial decrease in fluid electrical conductivity at the shallowest depth and the initial decrease in fluid electrical conductivity at greater depth.

The saturated hydraulic conductivity ($K_{sat}$) of the shallow riverbed sediments was determined using an integrated version of Darcy's law, to allow for the changing vertical hydraulic gradient during events, following:

$$K_{sat} = \frac{Z_{EC} n}{\sum_{i=1}^{N} \frac{dH}{dz}(t)\Delta t}$$

where, $Z_{EC}$ is the depth of the electrode in the riverbed, $n$ is an estimated porosity of 0.33 and $\sum_{i=1}^{N} \frac{dH}{dz}(t)\Delta t$ is the sum of the changing vertical hydraulic gradient time series over the measured time intervals $i$ to N, each of duration $\Delta t$.

## 3. Results

### 3.1. Long-Term Vertical Hydraulic Gradients (May 2012 to January 2014)

For 95% of the duration of the logged 21 month period, vertical hydraulic gradients were positive at site C (Figure 3). More than two thirds of the data had a strongly positive vertical hydraulic gradient (10–15%)

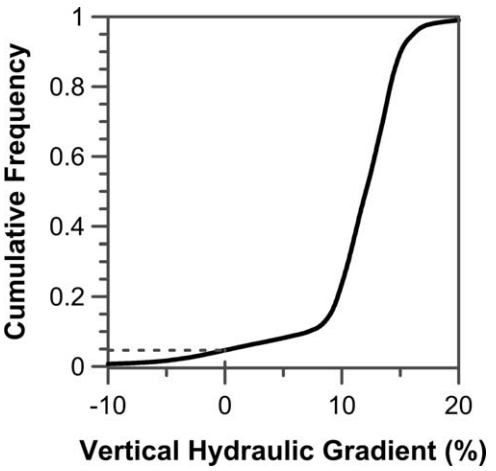


**Figure 3.** Cumulative frequency plot of vertical hydraulic gradients (%) at sampling site C, calculated between hydraulic head at 50 cm depth beneath the riverbed and stage, from May 2012 to January 2014. Dashed line marks the proportion of negative vertical hydraulic gradients. The vertical hydraulic gradient axis scale includes over 98% of data. The full vertical hydraulic gradient data range was −110% to +40%.

which equates to a 7.5 cm difference between the elevations of the riverbed hydraulic head and the stage. The mean increase in stage at the onset of a reversal in vertical hydraulic gradient was at least +0.55 m above the minimum stage for the duration of the logged period, although stage increases of +0.08 m and +1.77 m at the point when gradients changed were also recorded (Table 2).

The stable positive vertical gradient was present across the river (Figure 4). The mean vertical gradient was higher in the center of the channel (12.8%) than at the right (10.9%) and left channel locations (8.8%). The left channel location exhibited strongly reversed gradients in Summer-Winter 2012. Across the channel, vertical hydraulic gradients during 2012 were much more variable than those in 2013 (Figure 4), due to the greater frequency of high stage events during 2012 (Figure 2).

### 3.2. Large Magnitude Events (December 2013 to January 2014)

Focusing on a 7 week period between 4 December 2013 and 22 January 2014, there was a series of high stage events (Figure 5) resulting in repeated responses in riverbed fluid electrical conductivity. Figure 6 shows a typical response in vertical hydraulic gradients and fluid electrical conductivity ($EC_{25}$) in the riverbed across the channel at site C to an event that resulted in an increase in stage of more than 1 m. Event 4 (identified in Figure 5) was chosen to illustrate typical responses across the channel as there was a single peak with clear changes arising as a result of the rise in stage. Across the channel the vertical hydraulic gradients were stable and positive before the event, decreased and reversed during the peak of the event, and then reverted back to the same positive value after the event. Fluid EC decreased in response to the peak of the event and then returned to the stable value before the event. The left channel location showed the greatest decrease in vertical hydraulic gradient and a response in fluid EC was seen at both 20 and 30 cm depths beneath the riverbed. A higher positive vertical hydraulic gradient was observed in the central piezometer before the event; a moderated response to the event with a short period of reversal and no changes in logged fluid EC at any depth beneath the riverbed were also noted at this location. Vertical hydraulic gradient in the right channel piezometer reversed for the longest length of time but the reversed gradient was small and there was only a response in fluid EC at 10 cm depth beneath the riverbed.

Note that the estimated fluid EC values (as shown in Figure 6) are based on measured bulk EC and an assumed formation factor. From Figure 6, it can be seen that, even under preevent conditions, the interpreted fluid EC values vary across the channel and with depth. Such variation is likely to be a result of variation in porosity and sediment textural characteristics, i.e., variation in formation factor. For example, as porosity and formation factor are explicitly linked as shown in equation (3), an increase in porosity (e.g., in shallow sediments) will lead to a higher formation factor, and thus the interpreted fluid EC values will be greater. Nevertheless, assuming that porosity does not change throughout the event, then the changes in bulk EC will directly reflect the changes due to fluid EC alone. This is confirmed by the return to pre event EC values at the end of the event (as show for all series in Figure 6).

**Table 2.** Increase in Stage (m) Relative to Minimum Stage for the Period May 2012 to January 2014 (109.92 masl) at the Onset of Vertical Hydraulic Gradient Reversals at the Left, Center, and Right Channel Locations

| | Increase in Stage at Onset of Gradient Reversal (m) | | |
|---|---|---|---|
| | Mean (SD) | Minimum | Maximum |
| Left channel | +0.61 (0.25) | +0.22 | +1.16 |
| Center channel | +0.81 (0.38) | +0.24 | +1.77 |
| Right channel | +0.55 (0.28) | +0.08 | +1.34 |

The advective velocity of surface water infiltration into the subsurface, as a result of negative vertical hydraulic gradients, was calculated using the change in vertical

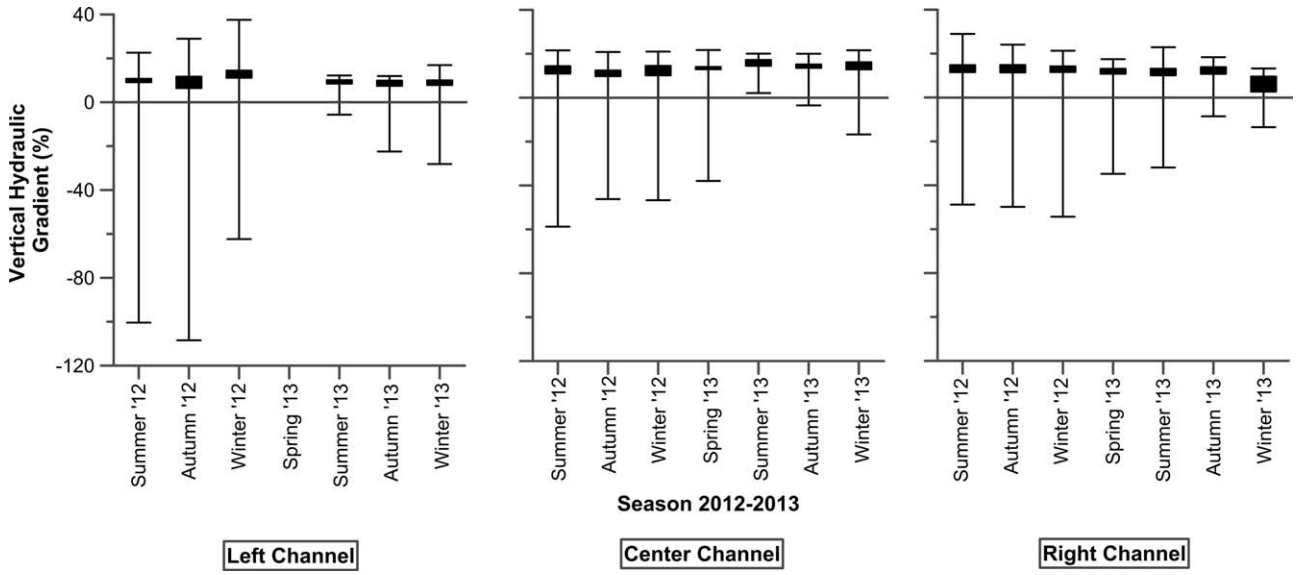


**Figure 4.** Box (interquartile range) and whisker (maximum and minimum) plots of vertical hydraulic gradients (%) by 3 month "season" period during 2012 and 2013 at the left, center, and right channel locations at sampling site C (Summer: June–August inclusive; Autumn: September–November inclusive; Winter: December–February inclusive; Spring: March–May inclusive). Blanks are missing data periods and the solid black line marks zero vertical hydraulic gradient.

hydraulic gradient and responses in subsurface fluid EC, as outlined in methods (section 2.3). During event 4 at the left channel location, the advective velocity between the riverbed surface and 20 cm depth was 13.0 cm/h, and between 20 and 30 cm depths was 4.4 cm/h (Figure 6 and Table 3). At the right channel location, the advective velocity between the riverbed surface and 10 cm depth was 1.7 cm/h (Figure 6). As highlighted above, there were no responses in fluid EC at any depths at the center channel location and therefore advective velocities were not calculated.

At the left channel location, the vertical hydraulic gradient and fluid EC responses to three further events, where the stage increased by more than 1 m, is explored in Figure 7. (left channel data are highlighted as this location displayed fluid EC responses to storm events at multiple depths in the subsurface). During each event, the vertical hydraulic gradient reversed to the same extent and then returned to the preevent value. The duration of the reversal in vertical gradient appears dependent on the length of time that elevated stage conditions are maintained, which is influenced by subsequent peaks in stage during the same event (Figure 7); peak stage level during events 2 and 3 were very similar (1.79 and 1.77 m above the low flow stage, respectively) but the rapid appearance of a second peak in stage in event 3 maintained the reversed gradient (Figure 7). Whereas, in event 2, there was sufficient time for recession of stage before the second peak leading to two reversals in vertical hydraulic gradient (Figure 7). Fluid EC consistently decreased in response to the events and then returned to the preevent value, apart from event 3 where, after the event, the fluid EC had apparently increased (Figure 7). This is likely to have been caused by scouring of the riverbed during event 3, resulting in the probes now representing a shallower depth in the subsurface (as noted earlier, changes in sediment textural characteristics and

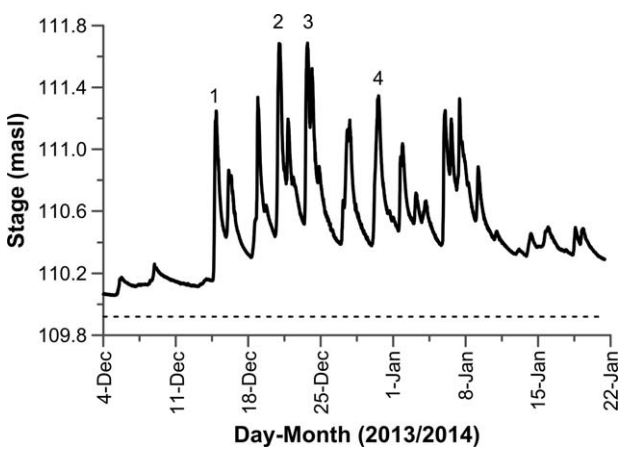


**Figure 5.** Stage (masl) in center of channel between the 4 December 2013 and the 22 January 2014 (7 weeks). Dashed line marks the minimum stage for the period May 2012 to Jan 2014 (109.92 masl). Numbers mark four events.

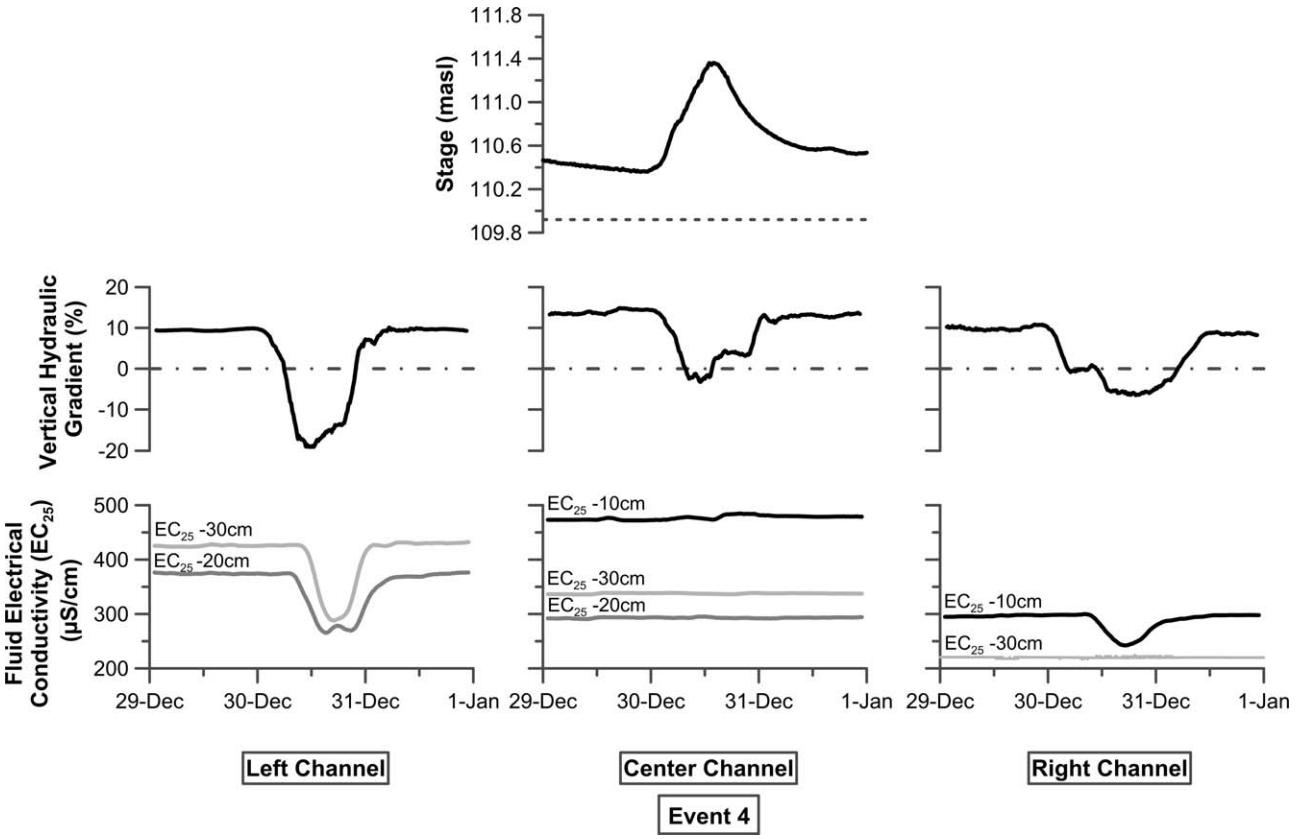


**Figure 6.** Stage (masl) and typical response of vertical hydraulic gradient (%), and riverbed fluid electrical conductivity ($EC_{25}$) ($\mu$S/cm) at the left, center, and right channel locations at sampling site C between 29 and 31st December 2013 (identified as event number 4 in Figure 5). Dates mark 00:00 hours at the start of each day. Vertical hydraulic gradients and fluid electrical conductivity are 3 h running averages. Missing fluid electrical conductivity data correspond to time periods when probes malfunctioned. Dashed line marks the minimum stage for the period May 2012 to January 2014 (109.92 masl). Dot-dash line marks zero vertical hydraulic gradient.

porosity surrounding the sensors will lead to changes in bulk EC and hence interpreted fluid EC). A decrease in the depth of the fluid EC probes is supported by the increase in fluid EC after event 3 (Figure 7).

At the left channel location, the advective velocities between the riverbed surface and 20 cm depth, and 20 cm to 30 cm depths were similar during events 1–3, with event 4 showing an elevated value between the surface and 20 cm depth (Table 3) as a result of the probes now representing shallower depths in the subsurface (as discussed above). The event 4 data are included in Table 3 to highlight the consistency in calculated advective velocities between the two subsurface depths.

**Table 3.** Left Channel Location Events 1–4 (Identified in Figure 5) Advective Velocities (cm/h) and Computed Saturated Hydraulic Conductivities (cm/h)[a]

| Event | Calculated Between Depths (cm) | Advective Velocity (cm/h) | Computed Saturated Hydraulic Conductivity (cm/h) |
|---|---|---|---|
| 1 | 0–20 | 4.4 | 10.8 |
| 2 | 0–20 | 5.0 | 10.8 |
| 3 | 0–20 | 4.2 | 8.3 |
| | 20–30 | 1.4 | |
| 4 | 0–20 | 13.0 | 18.0 |
| | 20–30 | 4.4 | |

[a]Advective velocities are derived from the time delay between the start of the reversed vertical hydraulic gradient and the first change in fluid electrical conductivity at depth, and the time delay between responses at multiple depths in the subsurface. Saturated hydraulic conductivities are computed from the time required for surface water infiltration into the riverbed to cause the first change in fluid electrical conductivity at depths under the reversed gradients, using an assumed porosity of 0.33.

The saturated hydraulic conductivity of the shallow riverbed sediments was calculated using the change in vertical hydraulic gradient and responses in subsurface fluid EC (equation (4)). Again, saturated hydraulic conductivity values were similar in events 1–3 and apparently elevated during event 4 as a result of the change in the representative depths of the electrodes, and consequent apparently faster response between the onset of the negative gradient and the initial response in fluid EC, at the left channel location (Table 3).

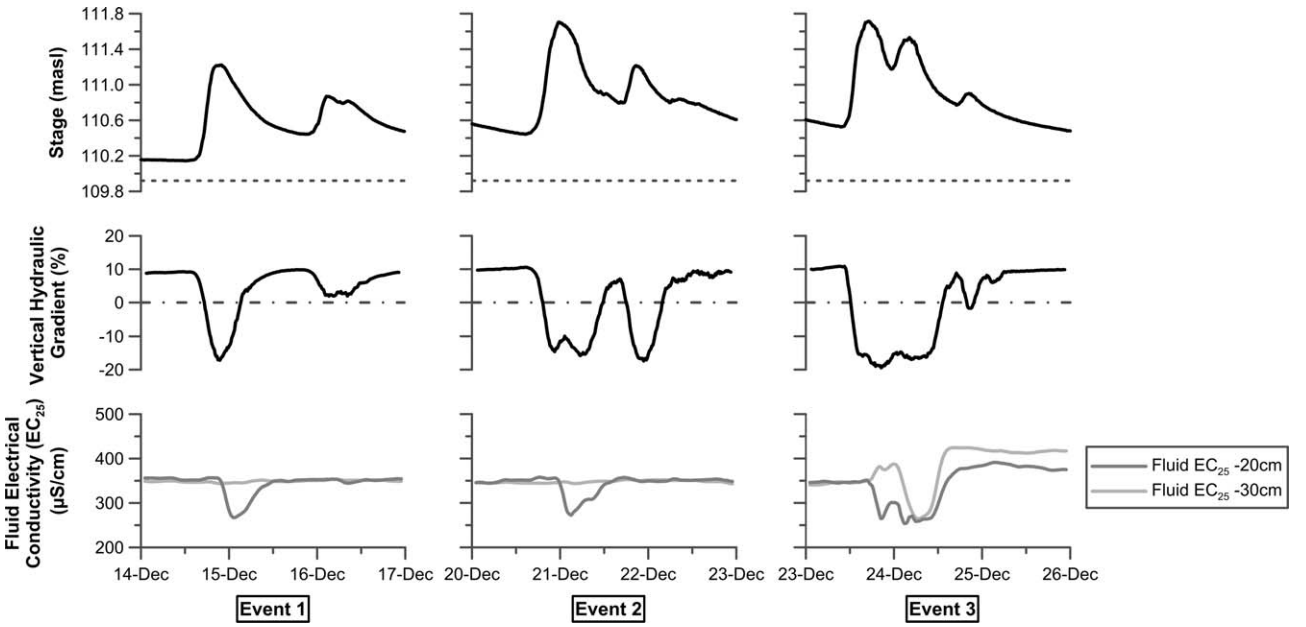


**Figure 7.** Stage (masl), vertical hydraulic gradient (%), and riverbed fluid electrical conductivity ($EC_{25}$) ($\mu$S/cm) at the left channel location at sampling site C during events 1–3 (identified in Figure 5). Dates mark 00:00 hours at the start of each day. Vertical hydraulic gradients and fluid electrical conductivity are 3 h running averages. Missing fluid electrical conductivity data correspond to time periods when probes malfunctioned. Dashed line marks the minimum stage for the period May 2012 to January 2014 (109.92 masl). Dot-dash line marks zero vertical hydraulic gradient.

### 3.3. Bank Flow Responses

The response of the shallow groundwater left bank flow bearing (i.e., direction) to river stage increases of more than 1 m, relative to minimum stage for the study period, is shown in Figure 8. Again event 4 is used to illustrate a typical response. The bearing decreases from a stable value of 233° (gradient 1.1%) before the event to 128° (gradient 5.0%) in response to the rise in surface stage. The bearing decreases because the piezometric head closest to the river rises faster than the piezometric heads observed further away from the river which show more moderated responses. The shallow groundwater bearing under high flow conditions is similar to the river flow direction as during these high stage peaks, the shallow groundwater piezometric heads and the river stage rise above the height of the riverbank and temporarily the river flows over the flooded banks, short circuiting part of the meander bend (Figure 1 and illustrated in Figure 9). As the peak in stage recedes, the bearing returns back to the preevent conditions, with the shallow groundwater flowing toward the river (Figure 8).

## Discussion

### 4.1. Control of Upwelling Groundwater

Previously *Binley et al*. [2013] identified the upstream area of the study site, centered around sampling location C, as an area of preferential groundwater discharge where vertical fluxes dominate and limit the mixing depth of surface water-groundwater interactions under low flow conditions. *Heppell et al*. [2014] estimated that between 4 and 9% of total in-stream nitrate transported through the reach in surface water is supplied from groundwater discharge within this area during base flow. The long-term occurrence of stable strong positive vertical gradients (Figures 3 and 4) and the rapid return to positive gradients following event-driven changes (Figure 7), highlighted in this study, support an area of strong groundwater upwelling at site C that limits vertical mixing between groundwater and surface water under low flow conditions, as also seen by *Lansdown et al*. [2014], *Binley et al*. [2013], and *Byrne et al*. [2014].

Considering small changes in stage (<40 cm) over a summer period at site C, *Byrne et al*. [2014] found that vertical gradients decreased, allowing hyporheic exchange flows to extend to 10 cm depth in the riverbed. We show that reversed vertical gradients can be generated at all times of the year (Figure 4) by a wide range of increases in stage (Table 2). The increase in stage at the start of a reversal in gradient, relative to

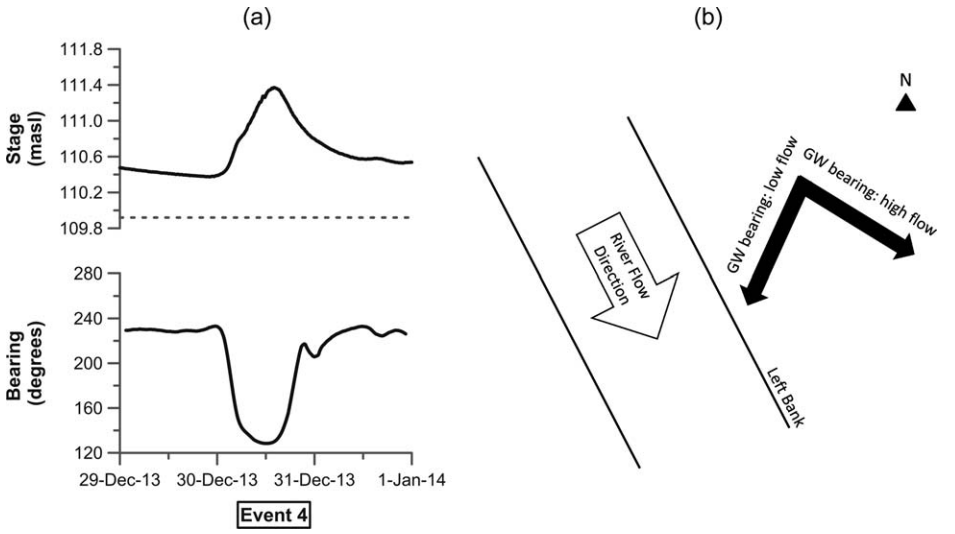


**Figure 8.** (a) Stage (masl) and typical response in shallow groundwater (50 cm beneath the adjacent riverbed) bearing (degrees) at the left bank of sampling site C during event 4 (identified in Figure 5). Dates mark 00:00 hours at the start of each day. Bearing is 3 h running average. Dashed line marks the minimum stage for the period May 2012 to January 2014 (109.92 masl) (b) Plan view conceptual model of shallow groundwater (GW) bearing change between high flows (128°) and low flows (233°) at sampling site C.

the low flow stage for the logged period, is dependent on the antecedent conditions at the site; a larger increase in stage is required to generate a reversed gradient during wet periods.

Considering changes in stage that exceed 1 m above the low flow stage, we show that the stable conditions at the site become temporarily altered with long duration reversals in vertical gradients increasing the mixing depth of surface water and shallow groundwater to at least 30 cm beneath the riverbed. The stability of vertical gradients and fluid electrical conductivity (EC) before event-driven changes, and the rapid return to the same values after events, reflects the dominance of the upwelling groundwater in this system. *Byrne et al*. [2014] speculated that the deeply incised channel morphology at site C creates a "bathtub" effect that acts to constrain the surface water within the channel causing it to rise quickly, leading to a reduction in vertical gradients. We show that reversed gradients can be generated with small changes in stage and persist even when surface water is no longer constrained within the channel and bankfull discharge is exceeded. Therefore, although channel morphology may play a role in driving gradient responses to events, as long as river stage rises faster and remains higher than subsurface hydraulic head, gradients will remain reversed. These conditions may arise as a result of variable catchment geology along the course of a stream

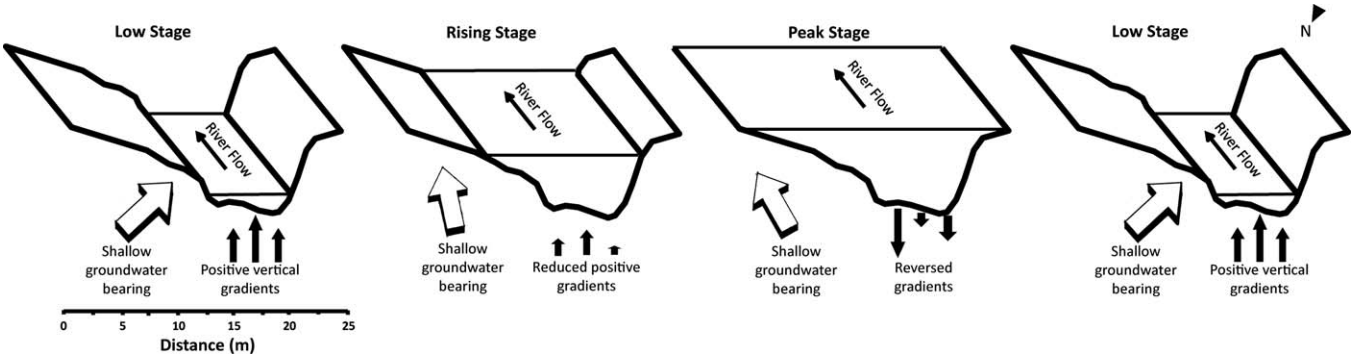


**Figure 9.** 3D cross-section conceptual model at sampling site C of shallow groundwater (50 cm beneath the adjacent riverbed) bearing (relative to North), and subchannel vertical hydraulic gradients (calculated between the hydraulic head 50 cm beneath the riverbed and the stage) during four points over the course of an event—low stage, rising stage, peak stage, and low stage. View is looking downstream from sampling site C. Unfilled arrows represent shallow groundwater bearing direction, filled arrows represent direction and magnitude of vertical hydraulic gradients.

where a flashy response in upstream areas will propagate downstream and may exceed local changes in groundwater response in the vicinity of the investigated reach.

### 4.2. Variability Across the Stream Channel

There is clear variability in responses across the channel, with the center of the channel consistently showing a moderated response in vertical gradient and no event-driven changes in fluid electrical conductivity. The distance from the channel margins (3.5 m) and consequently the reduced influence of lateral flows from riverbanks means that the upwelling groundwater head at 50 cm depth beneath the riverbed is greater in the center of the channel. Therefore, if there was a uniform increase in stage across the channel, the center of the channel would have a smaller reduction in vertical hydraulic gradient and the onset of a reversal in vertical gradient in the center channel location is generated under higher increases in stage (Table 2). Also, at the channel margin locations, as stage rises, the shallow riverbank groundwater flow direction turns away from entering the channel, further reducing the magnitude of restricting upwelling fluxes, allowing enhanced surface water downwelling. This finding is in contrast to *Zimmer and Lautz* [2014] who suggested that it is likely that the gradient toward the stream increases during the peak of an event, compressing the extent of the hyporheic zone. A schematic three-dimensional conceptual model of the combined responses in vertical gradients and bank flow direction in response to high stage levels is presented in Figure 9 and further develops the low flow conceptualization of the upper part of the field site [*Binley et al*., 2013].

### 4.3. Saturated Hydraulic Conductivity Derived From Advective Velocities

Our observations of fluid EC in the riverbed provide evidence of surface water infiltration in to the subsurface as a result of reversed hydraulic gradients during elevated stage conditions. *Malcolm et al*. [2004], *Sawyer et al*. [2009], and *Schmidt et al*. [2012] also interpreted decreases in fluid EC in hyporheic pore waters during high surface flows as an increasing surface water influence, and subsequent increased fluid EC during low flows as a decreasing surface water influence and increasing groundwater contributions. Unlike *Malcolm et al*. [2004] who conducted spot sampling of fluid EC, we have made use of continuous logging of riverbed fluid EC to evaluate responses to stage fluctuations of a magnitude that exceeds those that have previously been reported [*Schmidt et al*., 2012]. Previous work has determined advective travel times and estimated advective velocities using logged fluid EC along longitudinal pathways beneath in-stream gravel bars [*Schmidt et al*., 2012] or lateral infiltration into riverbanks [*Vogt et al*., 2010], but it is acknowledged that flow paths and location of infiltration are unknown if water table fluctuations in the river and aquifer are synchronous [*Vogt et al*., 2010]. By concurrently recording paired subsurface hydraulic head and stage at the same location as vertical profiles of subsurface fluid EC, we show that fluid EC fluctuations are attributable to observed vertical hydraulic gradient changes and can therefore calculate vertical advective velocities, rather than advective travel times.

The saturated hydraulic conductivity ($K_{sat}$) of shallow riverbed sediments was determined using the reversed vertical hydraulic gradient time series and the responses in subsurface fluid EC. The $K_{sat}$ values determined for the left channel location are very similar to the harmonic mean of $K_{sat}$ values determined using slug tests for piezometers at 20 and 50 cm depths beneath the riverbed at the left channel location (15.2 cm/h, unpublished data [*Binley et al*., 2013]). A comparison to the harmonic mean of $K_{sat}$ values at both 20 cm and 50 cm depths is required, as the vertical hydraulic gradient in this paper is based on the difference in hydraulic head between 50 cm depth beneath the riverbed and the surface and assumes that the head gradient is distributed instantaneously across the 50 cm vertical profile. Our values of $K_{sat}$ may be lower than the harmonic mean determined by *Binley et al*. [2013] as the values represent the effective $K_{sat}$ in the riverbed which includes potential clogging of riverbed sediment at shallow depths [*Schubert*, 2002].

The lower advective velocity seen at the right channel location would generate a lower $K_{sat}$ value than calculated at the left channel location. This is consistent with the observation of *Binley et al*. [2013] of slumping of riverbank sediments at the eroding side of the river, reducing $K_{sat.}$ We note that the $K_{sat}$ determinations are based on an assumed porosity that is uniform in the upper 50 cm, as in *Gerecht et al*. [2011], and we acknowledge that this is a simplification of the system as textural differences have been seen in riverbed cores from the site between these depths (refer to Figure 4, [*Binley et al*., 2013]).

These observed differences in calculated $K_{sat}$ between left and right channel locations emphasizes the control $K_{sat}$ has on water fluxes in to and out of the riverbed. *Kennedy et al*. [2009] noted that where high $K_{sat}$

was observed water flux was also high, but vertical hydraulic gradient was low. We show, in contrast, that responses in fluid EC across the channel are related to the duration and magnitude of vertical hydraulic gradient reversals even though $K_{sat}$ may be variable across the channel.

### 4.4. Implications of Observations for Hyporheic Zone Chemistry

Previous researchers have noted that induced surface water downwelling under weakened [*Byrne et al*., 2014] or reversed vertical gradients [*Gerecht et al*., 2011] will deliver high concentrations of dissolved organic carbon in to the riverbed, as well as sediment that contains a significant organic matter content [*Soulsby et al*., 2001]. *Kennedy et al*. [2009] observed that surface water infiltration into the riverbed around a beaver dam decreased subsurface nitrate concentrations which persisted beyond the point that the dam collapsed and infiltration ceased, suggesting reactants delivered by surface water may remain within the subsurface and continue to fuel nitrogen transformations.

Within a region of strong upwelling groundwater at the River Leith, a key question that previously remained unresolved was how surface-derived bioavailable organic matter might enter deeper bed sediments to drive denitrification, when chloride profiles indicated that under base flow conditions hyporheic exchange flow only penetrated to ~5cm depth. Here we show that a prolonged reversal in vertical head gradient can lead to an increase in mixing depth to at least 30 cm, and thus we have a mechanism by which dissolved organic carbon may be intermittently delivered to riverbed sediments to fuel denitrification.

Whereas the concurrent delivery of organic carbon, fine sediments and well-oxygenated surface water may initially support nitrification in the shallow riverbed, the microbial communities responsible for denitrification could, initially, be perturbed by the higher oxygen concentrations. Denitrification, however, does operate over a broad niche of reduced and oxygenated environments in a riverbed [*Lansdown et al*., 2014] and organic carbon delivered by hyporheic exchange processes during storm events may help drive denitrification once oxygen has been consumed in both a spatially and temporally distinct manner. For example, areas of net denitrification may be spatially distinct from zones of net nitrification along a downwelling flow path during periods of reversed gradients. Even when the positive vertical head gradient has re-established, and oxygen from surface waters has been consumed, degradation of ingressed organic matter that persists in the riverbed may still control denitrification. The persistence and relative importance of these mechanisms as a contribution to overall nitrate removal in the riverbed warrants further investigation.

Event-driven downwelling of surface water would not only change the chemistry of subsurface pore waters during the period of reversed gradients, but by increasing the residence time of upwelling groundwater, the extent of nitrate removal may also be increased [*Gu et al*., 2008b; *Gu et al*., 2008a]. *Zimmer and Lautz* [2014] hypothesized that denitrification was increased by both dissolved organic carbon delivery from a storm event and the longer residence time of pore waters in the subsurface. This highlights storm events as a potential time of increased reaction rate, by supply of reactants to the subsurface, and increased residence time which may act together to maximize nitrate removal in the riverbed. Considering hyporheic exchange in a lateral in-stream gravel bar where surface water nitrate concentrations were the same order of magnitude as seen at the Leith site, *Zarnetske et al*. [2011] saw net denitrification in hyporheic sediments beyond a threshold residence time of 6.9 h. The duration of the reversals in vertical hydraulic gradients and increased mixing depth highlighted in this paper all exceed this threshold time, and therefore it is likely that denitrification may be enhanced by the combined delivery of surface-borne reactive solutes to the hyporheic zone and increased hyporheic residence times.

Changes in lateral flow paths are also likely to enhance the residence time of subsurface waters originating from the stream. Our observations of changes in both vertical and lateral gradients and flow direction indicate a three-dimensional expansion of the hyporheic zone during events. These flow path fluctuations will alter the physical and chemical characteristics of the hyporheic zone, resulting in changes in biogeochemical processes, in an environment that would otherwise be dominated by groundwater composition [*Sawyer et al*., 2009].

In the UK, one of the predicted impacts of anticipated climate change is increased winter flows and more intense precipitation in winter months [*Rance et al*., 2012], generating more large magnitude changes in river stage. Over the 21 month observation period reported in this paper, vertical hydraulic gradients within the upstream part of the site, which is known to be dominated by upwelling groundwater, were reversed for 5% of the total time (Figure 3). An increase in mixing depth to 20 cm was seen when the gradient

reversal duration was in excess of 12 h (Event 1: Figure 7), which occurred in 22 events over the monitored period. More events with large changes in stage will increase the duration of reversed vertical gradients in gaining systems which may enhance denitrification in the hyporheic zone.

## 5. Conclusions

Building on multiple previous base flow studies at the River Leith site that have identified the upstream section of the reach as an area with predominantly upwelling flow, we have shown that storm events are a key driver of increased mixing depth between surface water and shallow groundwater in this gaining system. We highlight the use of logged fluid electrical conductivity as a natural tracer of mixing depth between surface water and groundwater in shallow riverbed sediments and its use to derive advective velocities and information on subsurface pore structure. We hypothesized that high river stage would increase the depth of mixing between surface water and groundwater by generating downwelling conditions. We have shown that prolonged vertical hydraulic gradient reversals, at the channel margins, allow surface water infiltration in to the subsurface, decreasing fluid electrical conductivity to depths of 30 cm and perhaps further. The mixing depth in the center of the channel seems to be maintained at less than 10 cm depth as there were only small change, short-duration reversals in vertical hydraulic gradient at this location. Considering the surrounding shallow aquifer, riverbank flow direction was also responsive to peak stage, aligning with the river flow direction when the riverbanks were flooded. This transition of lateral flow direction may lead to extensive (temporary) transfer of surface water to the riparian zone, enhancing the lateral expansion of the hyporheic zone during events.

The frequency and duration of changes in the mixing depth between surface water and groundwater shown in this study may fuel nitrate reduction processes that would otherwise be limited in systems dominated by upwelling flows. Biogeochemical reduction processes may be enhanced directly, by delivery of reactive solutes to the subsurface, and indirectly, by increasing the residence time of waters within the hyporheic zone. Considering the expected increase in the number of high stage events in the future as a consequence of anticipated changes in climate, it is likely that surface water-groundwater mixing will be enhanced in gaining systems, as a result of the mechanisms described in this paper, and event-driven changes will play a greater role in biogeochemical processes in the hyporheic zone. Consequently, characterization of processes under low flow conditions may be unrepresentative of the true function of this critical interface.

**Acknowledgments**

Data can be made available via the corresponding author. The site instrumentation and setup was funded by NERC grant NE/F006063/1. This work was funded by NERC PhD studentship NE/I527953/1. This paper contains Environment Agency information © Environment Agency and database right. We thank Sarah Barr, Vassil Karloukovski, Lakam Mejus, and Peter Shanahan for their valued assistance with fieldwork. We also thank Catherine Heppell for comments that helped strengthen the manuscript.

## References

Archie, G. E. (1942), The electrical resistivity log as an aid in determining some reservoir characteristics, *Trans. Am. Inst. Min. Metall. Pet. Eng.*, *146*, 54–62.

Arntzen, E. V., D. R. Geist, and P. E. Dresel (2006), Effects of fluctuating river flow on groundwater/surface water mixing in the hyporheic zone of a regulated, large cobble bed river, *River Res. Appl.*, *22*, 937–946, doi:10.1002/rra.947.

Baker, M. A., C. N. Dahm, and H. M. Valett (1999), Acetate retention and metabolism in the hyporheic zone of a mountain stream, *Limnol. Oceanogr.*, *44*, 1530–1539.

Binley, A., and A. Kemna (2005), Electrical methods, in *Hydrogeophysics*, edited by Y. Rubin and S. Hubbard, pp. 129–156, Springer, Dordrecht, Netherlands.

Binley, A., S. Ullah, A. L. Heathwaite, C. Heppell, P. Byrne, K. Lansdown, M. Trimmer, and H. Zhang (2013), Revealing the spatial variability of water fluxes at the groundwater-surface water interface, *Water Resour. Res.*, *49*, 3978–3992, doi:10.1002/wrcr.20214.

Boano, F., R. Revelli, and L. Ridolfi (2008), Reduction of the hyporheic zone volume due to the stream-aquifer interaction, *Geophys. Res. Lett.*, *35*, L09401, doi:10.1029/2008GL033554.

Briggs, M. A., L. K. Lautz, J. M. McKenzie, R. P. Gordon, and D. K. Hare (2012), Using high-resolution distributed temperature sensing to quantify spatial and temporal variability in vertical hyporheic flux, *Water Resour. Res.*, *48*, W02527, doi:10.1029/2011WR011227.

Butcher, A. S., A. R. Lawrence, C. Jackson, J. Cunningham, E. Cullis, and K. H. J. Ingram (2003), *Investigations of Rising Nitrate Concentrations in Groundwater in the Eden Valley, Cumbria: Phase 1 Project Scoping Study*, pp. 1–71, Environ. Agency, Bristol, U. K.

Byrne, P., A. Binley, A. L. Heathwaite, S. Ullah, C. M. Heppell, K. Lansdown, H. Zhang, M. Trimmer, and P. Keenan (2014), Control of river stage on the reactive chemistry of the hyporheic zone, *Hydrol. Processes*, *28*, 4766–4779, doi:10.1002/hyp.9981.

Cardenas, M. B., and M. S. Markowski (2010), Geoelectrical imaging of hyporheic exchange and mixing of river water and groundwater in a large regulated river, *Environ. Sci. Technol.*, *45*, 1407–1411, doi:10.1021/es103438a.

Cardenas, M. B., and J. L. Wilson (2007), Exchange across a sediment–water interface with ambient groundwater discharge, *J. Hydrol.*, *346*, 69–80, doi:10.1016/j.hydrol.2007.08.019.

Cirpka, O. A., M. N. Fienen, M. Hofer, E. Hoehn, A. Tessarini, R. Kipfer, and P. K. Kitanidis (2007), Analyzing bank filtration by deconvoluting time series of electric conductivity, *Ground Water*, *45*, 318–328, doi:10.1111/j.1745-6584.2006.00293.x.

Fritz, B. G., and E. V. Arntzen (2007), Effect of rapidly changing river stage on uranium flux through the hyporheic zone, *Ground Water*, *45*, 753–760, doi:10.1111/j.1745-6584.2007.00365.x.

Genereux, D. P., S. Leahy, H. Mitasova, C. D. Kennedy, and D. R. Corbett (2008), Spatial and temporal variability of streambed hydraulic conductivity in West Bear Creek, North Carolina, USA, *J. Hydrol.*, *358*, 332–353, doi:10.1016/j.hydrol.2008.06.017.

Gerecht, K. E., M. B. Cardenas, A. J. Guswa, A. H. Sawyer, J. D. Nowinski, and T. E. Swanson (2011), Dynamics of hyporheic flow and heat transport across a bed-to-bank continuum in a large regulated river, *Water Resour. Res.*, *47*, W03524, doi:10.1029/2010WR009794.

Gu, C., G. M. Hornberger, J. S. Herman, and A. L. Mills (2008a), Effect of freshets on the flux of groundwater nitrate through streambed sediments, *Water Resour. Res.*, *44*, W05415, doi:10.1029/2007WR006488.

Gu, C., G. M. Hornberger, J. S. Herman, and A. L. Mills (2008b), Influence of stream-groundwater interactions in the streambed sediments on $NO_3^-$ flux to a low-relief coastal stream, *Water Resour. Res.*, *44*, W11432, doi:10.1029/2007WR006739.

Harvey, J. W., B. J. Wagner, and K. E. Bencala (1996), Evaluating the reliability of the stream tracer approach to characterize stream-subsurface water exchange, *Water Resour. Res.*, *32*, 2441–2451, doi:10.1029/96WR01268.

Hayashi, M. (2004), Temperature-electrical conductivity relation of water for environmental monitoring and geophysical data inversion, *Environ. Monit. Assess.*, *96*, 119–128, doi:10.1023/B:EMAS.0000031719.83065.68.

Heppell, C., A. Louise Heathwaite, A. Binley, P. Byrne, S. Ullah, K. Lansdown, P. Keenan, M. Trimmer, and H. Zhang (2014), Interpreting spatial patterns in redox and coupled water–nitrogen fluxes in the streambed of a gaining river reach, *Biogeochemistry*, *117*, 491–509, doi:10.1007/s10533-013-9895-4.

Holmes, R., J. Jones Jr., S. Fisher, and N. Grimm (1996), Denitrification in a nitrogen-limited stream ecosystem, *Biogeochemistry*, *33*, 125–146, doi:10.1007/BF02181035.

Johnson, T. C., L. Slater, D. Ntarlagiannis, F. D. Day-Lewis, and M. Elwaseif (2012), Monitoring groundwater-surface water interaction using time-series and time-frequency analysis of transient three-dimensional electrical resistivity changes, *Water Resour. Res.*, *48*, W07506, doi:10.1029/2012WR011893.

Käser, D. H., A. Binley, A. L. Heathwaite, and S. Krause (2009), Spatio-temporal variations of hyporheic flow in a riffle-step-pool sequence, *Hydrol. Processes*, *23*, 2138–2149, doi:10.1002/hyp.7317.

Kennedy, C. D., D. P. Genereux, D. R. Corbett, and H. Mitasova (2009), Spatial and temporal dynamics of coupled groundwater and nitrogen fluxes through a streambed in an agricultural watershed, *Water Resour. Res.*, *45*, W09401, doi:10.1029/2008WR007397.

Krause, S., F. Boano, M. O. Cuthbert, J. H. Fleckenstein, and J. Lewandowski (2014), Understanding process dynamics at aquifer-surface water interfaces: An introduction to the special section on new modeling approaches and novel experimental technologies, *Water Resour. Res.*, *50*, 1847–1855, doi:10.1002/2013WR014755.

Lansdown, K., M. Trimmer, C. M. Heppell, F. Sgouridis, S. Ullah, A. L. Heathwaite, A. Binley, and H. Zhang (2012), Characterization of the key pathways of dissimilatory nitrate reduction and their response to complex organic substrates in hyporheic sediments, *Limnol. Oceanogr.*, *57*, 387–400, doi:10.4319/lo.2012.57.2.0387.

Lansdown, K., C. M. Heppell, M. Dossena, S. Ullah, A. L. Heathwaite, A. Binley, H. Zhang, and M. Trimmer (2014), Fine-scale in situ measurement of riverbed nitrate production and consumption in an armored permeable riverbed, *Environ. Sci. Technol.*, *48*, 4425–4434, doi:10.1021/es4056005.

Malcolm, I. A., C. Soulsby, A. F. Youngson, D. M. Hannah, I. S. McLaren, and A. Thorne (2004), Hydrological influences on hyporheic water quality: Implications for salmon egg survival, *Hydrol. Processes*, *18*, 1543–1560, doi:10.1002/hyp.1405.

Malcolm, I. A., C. Soulsby, and A. F. Youngson (2006), High-frequency logging technologies reveal state-dependent hyporheic process dynamics: Implications for hydroecological studies, *Hydrol. Processes*, *20*, 615–622, doi:10.1002/hyp.6107.

McClain, M. E., E. W. Boyer, C. L. Dent, S. E. Gergel, N. B. Grimm, P. M. Groffman, S. C. Hart, J. W. Harvey, C. A. Johnston, and E. Mayorga (2003), Biogeochemical hot spots and hot moments at the interface of terrestrial and aquatic ecosystems, *Ecosystems*, *6*, 301–312, doi:10.1007/s10021-003-0161-9.

Osenbrück, K., T. Wöhling, D. Lemke, N. Rohrbach, M. Schwientek, C. Leven, C. Castillo Alvarez, H. Taubald, and O. Cirpka (2013), Assessing hyporheic exchange and associated travel times by hydraulic, chemical, and isotopic monitoring at the Steinlach Test Site, Germany, *Environ. Earth Sci.*, *69*, 359–372, doi:10.1007/s12665-012-2155-4.

Rance, J., S. D. Wade, A. P. Hurford, E. Bottius, and N. S. Reynard (2012), *Climate Change Risk Assessment for the Water Sector*, Dep. for Environ., pp. 1–129, Food and Rural Affairs, London, U. K.

Sawyer, A., L. Kaplan, O. Lazareva, and H. Michael (2014), Hydrologic dynamics and geochemical responses within a floodplain aquifer and hyporheic zone during Hurricane Sandy, *Water Resour. Res.*, *50*, 4877–4892, doi:10.1002/2013WR015101.

Sawyer, A. H., M. B. Cardenas, A. Bomar, and M. Mackey (2009), Impact of dam operations on hyporheic exchange in the riparian zone of a regulated river, *Hydrol. Processes*, *23*, 2129–2137, doi:10.1002/hyp.7324.

Schmidt, C., A. Musolff, N. Trauth, M. Vieweg, and J. H. Fleckenstein (2012), Transient analysis of fluctuations of electrical conductivity as tracer in the stream bed, *Hydrol. Earth Syst. Sci.*, *16*, 3689–3697, doi:10.5194/hess-16-3689-2012.

Schubert, J. (2002), Hydraulic aspects of riverbank filtration: Field studies, *J. Hydrol.*, *266*, 145–161, doi:10.1016/S0022-1694(02)00159-2.

Sorensen, J. A., and G. E. Glass (1987), Ion and temperature dependence of electrical conductance for natural waters, *Anal. Chem.*, *59*, 1594–1597, doi:10.1021/ac00140a003.

Soulsby, C., I. A. Malcolm, and A. F. Youngson (2001), Hydrochemistry of the hyporheic zone in salmon spawning gravels: A preliminary assessment in a degraded agricultural stream, *Reg. Rivers Res. Manage.*, *17*, 651–665, doi:10.1002/rrr.625.

Stelzer, R. S., and L. A. Bartsch (2012), Nitrate removal in deep sediments of a nitrogen-rich river network: A test of a conceptual model, *J. Geophys. Res.*, *117*, G02027, doi:10.1029/2012JG001990.

Unland, N. P., I. Cartwright, M. S. Andersen, G. C. Rau, J. Reed, B. S. Gilfedder, A. P. Atkinson, and H. Hofmann (2013), Investigating the spatiotemporal variability in groundwater and surface water interactions: A multi-technique approach, *Hydrol. Earth Syst. Sci.*, *17*, 3437–3453, doi:10.5194/hess-17-3437-2013.

Vogt, T., E. Hoehn, P. Schneider, A. Freund, M. Schirmer, and O. A. Cirpka (2010), Fluctuations of electrical conductivity as a natural tracer for bank filtration in a losing stream, *Adv. Water Resour.*, *33*, 1296–1308, doi:10.1016/j.advwatres.2010.02.007.

Ward, A. S., M. N. Gooseff, and K. Singha (2010a), Characterizing hyporheic transport processes: Interpretation of electrical geophysical data in coupled stream–hyporheic zone systems during solute tracer studies, *Adv. Water Resour.*, *33*, 1320–1330, doi:10.1016/j.advwatres.2010.05.008.

Ward, A. S., M. N. Gooseff, and K. Singha (2010b), Imaging hyporheic zone solute transport using electrical resistivity, *Hydrol. Processes*, *24*, 948–953, doi:10.1002/hyp.7672.

Ward, A. S., M. Fitzgerald, M. N. Gooseff, T. J. Voltz, A. M. Binley, and K. Singha (2012), Hydrologic and geomorphic controls on hyporheic exchange during base flow recession in a headwater mountain stream, *Water Resour. Res.*, *48*, W04513, doi:10.1029/2011WR011461.

Zarnetske, J. P., R. Haggerty, S. M. Wondzell, and M. A. Baker (2011), Dynamics of nitrate production and removal as a function of residence time in the hyporheic zone, *J. Geophys. Res.*, *116*, G01025, doi:10.1029/2010JG001356.

Zimmer, M. A., and L. K. Lautz (2014), Temporal and spatial response of hyporheic zone geochemistry to a storm event, *Hydrol. Processes*, *28*, 2324–2337, doi:10.1002/hyp.9778.